EASR

Engineering and Applied Science Research

https://www.tci-thaijo.org/index.php/easr/index

Published by the Faculty of Engineering, Khon Kaen University, Thailand

Integrated neural network-based MPPT and ant colony optimization-tuned PI bidirectional charger-controller for PV-powered motor-pump system

Rati Wongsathan*

Department of Electrical Engineering, Faculty of Engineering and Technology, North-Chiang Mai University, Chiang Mai 50230, Thailand

Received 4 July 2024
Revised 2 August 2024
Accepted 21 August 2024

Abstract

This study presents the design and implementation of an efficient off-grid photovoltaic (PV)-powered motor-pump system utilizing a two-stage power converter. The system integrates a neural network-based maximum power point tracking (MPPT-NN) algorithm with a proportional integral (PI) controller and an additional bidirectional PI charger. Controller gains are optimized using ant colony optimization (ACO) to achieve optimal performance. The proposed MPPT-NN-PI/ACO controller enhances control responses and improves energy utilization efficiency by 17% compared to traditional PI controller. Performance comparisons of MPPT techniques demonstrates that the proposed controller outperforms several existing methods, including commercial on-off controllers, the modified Perturb & Observe algorithm, and neural network-based controllers, by approximately 4%–20%. It shows a slightly different performance of about 1%–6% compared to advanced adaptive controllers, including fuzzy logic and neuro-fuzzy controllers. For bidirectional charger performance, the DC bus voltage connecting the boost converter and bidirectional converter remains stable with small ripples and is well-aligned with the reference voltage, ensuring uninterrupted operation under varying weather conditions. The bidirectional charge management effectively maintains battery state-of-charge (SOC), showing a decline during periods of insufficient PV energy and achieving full charging during periods of excess PV energy. System performance is validated through both simulation and laboratory-scale prototyping, ensuring robust operation.

Keywords: ACO, Bidirectional charger, MPPT, Neural networks, Photovoltaic pumping system

1. Introduction

In workplaces lacking grid connectivity or facing high diesel fuel costs, adopting photovoltaic (PV)-powered water pumping systems (PVWPS) is crucial for ensuring a reliable water supply [1-7]. Integrating batteries into these systems enables uninterrupted operation throughout day and night cycles, requiring a specific number of solar panels to store energy while simultaneously driving the motor-pump. However, this integration significantly increases the overall system cost, and the reduced PV conversion efficiency poses a major drawback for PV applications, particularly in PV-powered motor-pump systems [3].

Typically, users with limited capital and less knowledge in PV technology tend to favor straightforward systems, such as directly connecting solar panels to motor-pumps or batteries without any power electronic-based controller or charger. While this approach significantly reduces initial costs, it also decreases output PV power, thereby reducing PV energy utilization efficiency and leading to overall system performance degradation. Furthermore, this practice can raise maintenance costs due to heat from PV power fluctuations and shorten the lifespan of components. The nonlinear and weather-dependent PV voltage-current characteristics further limits the full capacity of PV systems when supplying power to motor-pump applications. This results in output power deviations from the maximum power points (MPP) that should be achieved. Such deviations, caused by variations in solar irradiance and ambient temperature, affect the efficiency and performance of the PV motor-pump system, preventing it from consistently operating at optimal power output levels. Consequently, the system may experience performance fluctuations, reducing overall system reliability and effectiveness.

To address these challenges comprehensively in engineering design while considering limited budget constraints, minimizing PV panel sizing is crucial. This involves using a boost converter with a maximum power point tracking (MPPT)-based controller to step up the low PV voltage to a higher set voltage, while ensuring the operating point remains near the MPP under various weather conditions [8]. In [5], a multilevel high-gain boost converter with additional diodes and capacitors, yet retaining only one switch, is proposed. This configuration can reduce switch stress and ripple compared to conventional boost converters.

In literature, various topologies of DC-DC converters are employed for extensive MPPT performance, such as SEPIC [4], ZETA [9, 10], CUK [4], Luo [2], and others. Among these, the Luo converter outperforms the rest in terms of very low voltage/current ripple and high-power density with acceptable cost [2]. Recently, the hybrid CUK-SEPIC converter proposed by [4] demonstrates an advanced topology by integrating the input and output magnetic cores of the inductor, minimizing ripple current and thereby optimizing the extracted MPP, compared to conventional CUK and SEPIC converters.

*Corresponding author.
Email address: rati@northcm.ac.th; rati1003@gmail.com
doi: 10.14456/easr.2024.57

Consequently, MPP trackers are essential tools that have been extensively discussed in the literature. Although classical MPPT algorithms such as perturb and observe (P&O), incremental conductance (INC), hill climbing (HC), short circuit current, open circuit voltage, and others are commonly used due to their simplicity and ease of hardware implementation [11], their transient and steady-state performance depends on the selected perturbation size. The hardware implementation of P&O and HC tends to result in low efficiency due to the power losses from high oscillations occurring near the MPP [9]. To overcome the limitations of the fixed step size in conventional P&O, the modulated P&O (MoP&O) is proposed [12]. This approach utilizes a modulated step size, reducing it during steady-state conditions to minimize oscillations and increasing it during rapid changes in irradiance to quickly track the new MPP. In [13], the single-input adaptive fuzzy-logic tuned P&O (SFPO) MPPT algorithm is introduced, addressing the fixed step-change issues of the classical P&O MPPT technique. The adaptive step size-based MPPT, such as the weight of set point similarity (WSPS) proposed under uniformly shaded conditions in [6], is superior to the modified P&O (MP&O) and enhanced INC methods, which rely on a scaling factor depending on the power rating of the used PV panel. For optimal MPPT performance, adaptive controllers such as neural network (NN) [14], fuzzy logic controller (FLC) [3, 5, 10, 15, 16], and adaptive neuro-fuzzy inference system (ANFIS)-based controller (a hybrid of NN and FLC) [7, 9, 17] are preferred due to their ability to achieve MPP quickly with zero oscillation during tracking.

In this regard, the FLC with multiple control rules has a simpler mechanism to tackle the nonlinear and uncertain nature of PV power applications, whereas the NN consisting of multiple layer nonlinear processing, provides fast tracking under rapid weather changes. Typically, two configurations of FLC are applied for MPPT in PV applications. The Takagi-Sugeno fuzzy logic controller (TS-FLC)-based MPPT offers faster tracking to the MPP and ensures stability for PV-powered water pumping systems, with less complexity and reduced computation time compared to the conventional Mamdani fuzzy logic control (M-FLC)-based MPPT [3]. However, designing fuzzy rules and parameters is a challenging task, usually relying on trial-and-error human tuning, which may not achieve optimal MPPT performance. In [18, 19], this issue can be addressed using a multi-objective genetic algorithm (MOGA). In this approach, all fuzzy rules and parameters are encoded in artificial chromosomes. The optimal solution (the best chromosome), determined through genetic operators, i.e., mutation and crossover, is selected based on two criteria: minimizing the steady-state error of MPPT and simultaneously reducing redundant fuzzy rules. This results in decreased complexity and optimized control performance. In [16], the single input adaptive fuzzy logic tuned with deterministic optimization (SIAFL-DO) is proposed, which accurately executes MPPT and is implemented in a hardware prototype. The NN-based controller (NNC) is proposed by [20] also faces challenges, as NN requires large training data and is prone to overfitting. The NNC's structure can be optimized using a hybrid MOGA and back-propagation algorithm (*h*MOGA/BPA), which enhances MPPT performance. The ANFIS controller shows the best performance compared to FLC and NN [19], despite their greater computational complexity.

The MPPT-based optimized techniques using population search for the global MPPT (GMPPT) under partial shading conditions that cause multi-peak power have been developed, including genetic algorithm (GA), artificial bee colony (ABC), firefly algorithm (FA), human psychology optimization (HPO), gravitational search algorithm (GSA), grey wolf optimization (GWO), and particle swarm optimization (PSO). According to [2], a modified FA outperforms P&O and PSO in terms of tracking under transient weather conditions and exhibits lower complexity. For GMPPT-based HPO [21], reducing the population size, a significant parameter, suppresses computation burden and constraints, thereby improving both dynamic and steady-state conditions, which other methods cannot achieve simultaneously. This makes HPO particularly suitable for implementation using microcontroller. Alternatively, the hybrid GSA-PSO-based MPPT proposed by [4] is highly effective in achieving MPP, demonstrating high convergence velocity and better accuracy. Recent advancements also include the use of hybrid CUK-SEPIC converters [4], thereby optimizing the extracted MPP. In recent advancements [22], a hybrid whale optimization algorithm-differential evolution (WOADE) has been proposed as a MPPT technique for wind energy conversion systems (WECS) used in water pumping applications. This novel hybrid MPPT algorithm ensures swift and oscillation-free power tracking, achieving the GMPP within a limited number of iterations.

Various DC and AC motor-driven systems have been employed in PV-powered water pumping applications. Typically, permanent magnet DC (PMDC) motors are the most popular choice for small-scale PV pumping systems due to their direct coupling with PV modules, which eliminates the need for additional power electronics. However, these systems suffer from low efficiency and high maintenance costs, which are significant drawbacks [4]. Permanent magnet AC (PMAC) motors, although frequently used in the agricultural sector, are often more expensive [3]. On the other hand, induction motors (IMs) are predominantly used in PV pumping systems due to their robustness, reliable operation, and cost-effectiveness. For a PV pumping system using IM, a three-tiered fuzzy-predictive controller for the bidirectional charger, boost converter, and inverter-coupled IM [23] enhances MPPT performance and reduces ripples compared to P&O, PI, and conventional torque control. However, this results in significant computational complexity.

In scenarios where a PV water pumping system requires 24-hour operation, particularly in the agricultural sector, a bidirectional converter is employed to efficiently manage battery charging and discharging, storing excess energy for low sunlight periods or nighttime operation of the motor-pump. For a grid-interactive PV pumping system, a smart bidirectional converter controlled by MPPT-IC and PI controllers is used to manage the flow of PV energy to batteries [24]. This approach reduces electricity costs for the user; however, the MPPT response and power quality remain suboptimal. For off-grid PV pumping systems, various MPPT and bidirectional charger algorithms have been proposed [25]. Due to their simplicity and ease of implementation, these applications predominantly use PI controllers. However, identifying an optimal set of PI gains is a challenging task. Using exhaustive trial-and-error method or traditional approaches based on selecting the damping ratio of quadratic equations, which typically result in fixed PI gains, performs well only within limited operational range. Adaptive PI gains are preferred for uncertain PV systems [26], but they require fast processing units that may not always respond promptly to system changes. Alternatively, to enhance control performance in PV-pumping system, optimized PI controllers are achieved using bio-inspired techniques, such as the water cycle algorithm (WCA) [27], Jellyfish optimizer [25], PSO [26, 28], GA [28], and BAT [28].

This study aims to design an efficient off-grid PV-powered motor-pump system with battery storage for continuous operation under environment changes. The system utilizes a brushless direct current (BLDC) motor driving a centrifugal pump, maintaining constant speed and good alignment with tracked MPPs, and employs Lithium-ion batteries for their fast-charging advantage. To ensure reliability and cost-effectiveness, sizing system involves stepping PV voltage up using a boost converter and managing charging through a bidirectional converter. Overall system efficiency is enhanced by designing converter circuits and integrating MPPT-NN with PI controller in the boost stage, along with an additional PI controller in the bidirectional charging stage. PI gains are tuned using ACO [29], most used technique, for superior performance. MATLAB/Simulink simulations are conducted, and a laboratory-scale prototype is implemented for validation. The efficiency of the proposed controllers is demonstrated by evaluating MPPT dynamics, power fluctuations, voltage-current ripple reduction, DC-bus voltage control, motor speed and torque control, and charge performance compared to other controllers.

Despite advancements in PV-powered water pumping systems, several challenges remain unaddressed, particularly in optimizing system efficiency and cost-effectiveness. This study aims to address these issues by identifying key research gaps and proposing solutions to enhance the overall performance of off-grid PV-powered motor-pump systems.

1) Integrating batteries in PV-powered motor-pump systems increases costs and reduces PV conversion efficiency. Simple systems without controllers lead to decreased energy utilization and overall performance.
2) Classical MPPT methods like P&O suffer from efficiency losses due to oscillations near the MPP. Advanced algorithms (e.g., GA, PSO) improve performance but introduce significant computational complexity.
3) Designing FLC involves complex, trial-and-error tuning. NNC require extensive training data and risk overfitting, complicating their practical application.
4) Existing bidirectional charge management systems are not optimized for continuous 24-hour PV water pumping, leading to suboptimal MPPT response and power quality.

To address these research gaps, this study develops an innovative off-grid PV-powered motor-pump system. The following major contributions and findings demonstrate the effectiveness and advancements of the proposed approach.

1) The integration of the neural network-based MPPT-NN algorithm with a PI controller and ACO tuned bidirectional charger-controller significantly enhances energy utilization efficiency. The proposed MPPT-NN-PI/ACO controller improves energy utilization efficiency by 17% compared to traditional tuning methods.
2) The proposed MPPT-NN-PI/ACO controller demonstrates superior control performance over several existing methods. It outperforms commercial on-off controllers, MP&O algorithm, and NNC by approximately 4%–20%. The performance is also slightly different, by about 1%–6%, when compared to FLC and NFC.
3) The DC bus voltage connecting the boost converter and bidirectional converter remains stable with minimal ripples, ensuring uninterrupted operation under varying weather conditions. This stability is crucial for maintaining the continuous and efficient operation of the motor-pump system.
4) The bidirectional charge management system effectively maintains the battery state-of-charge (SOC). It ensures a decline in SOC during periods of insufficient PV energy and achieves full charging during periods of excess PV energy, thereby optimizing battery usage and extending the lifespan of the battery.
5) The system performance is validated through both simulation and laboratory-scale prototyping. This comprehensive validation ensures the robustness of the proposed system, demonstrating its practical applicability and reliability in real-world scenarios.

2. System design

The proposed PV pumping system (Figure 1) comprises a BLDC motor driving a pump (24 W, 24 V, max current: 1 A) requiring about 600 Wh of total energy (250 Wh in daytime and 350 Wh in night-time). Powered by a 130 W PV panel (P_{rated}), operating 7 hours daily, resulting under 900 Wh energy output, subject to solar irradiance (G) and temperature (T) conditions. Surplus energy (≈650 Wh) is used for battery charging, which are supported by two series connected 15 Ah 12 V batteries.

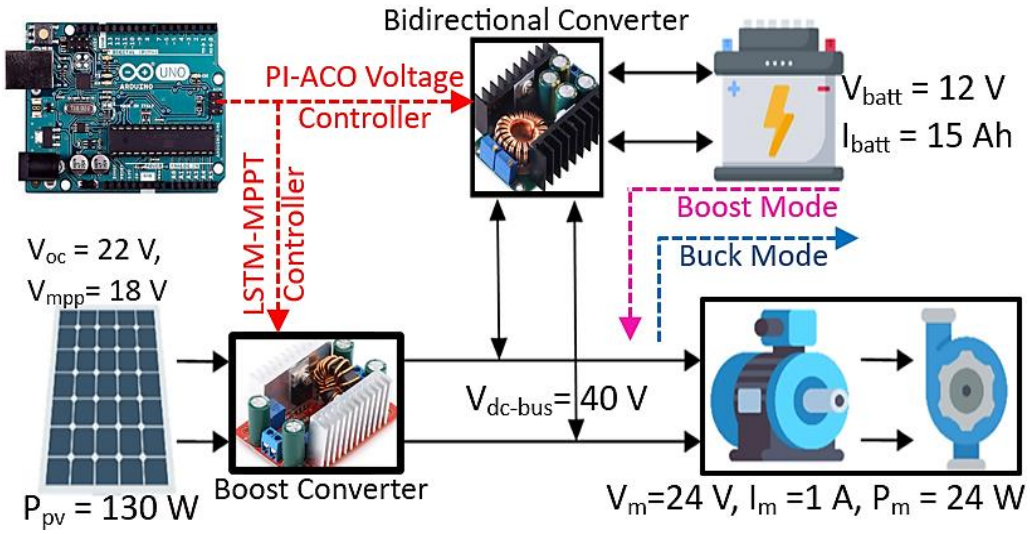

Figure 1 PV pumping system with the proposed controllers

The DC bus output voltage is stepped up to 40 V (V_{out}) using boost converter (Figure 2), requiring a minimum inductance ($L_{min,boost}$) and capacitance ($C_{min,boost}$) as outlined in (1) and (2), respectively [30]. These values are determined based on the required minimum ripple current (ΔI_{ripple}) for the inductor, and ripple voltage (ΔV_{ripple}) for the capacitor.

To validate $L_{min,boost}$, the increasing rate of ripple current ($\Delta I_{ripple}/D\times T_s$) during the switch-on period ($D\times T_s$) is given by $V_{in}/L_{min,boost}$ (dI_L/dt), where V_{in} is the input PV voltage, I_L is the inductor current, T_s is the period of single pulse width modulated (PWM) signal and D is the duty ratio. For $C_{min,boost}$, the conservation of charge principle applies: the increase in charge during the switch-on period ($\Delta Q = D\times T_s\times V_{out}/R_{Load}$) is equal to the charge change during the switch-off period ($\Delta Q = C_{min,boost}\times\Delta V_{ripple}$), where R_{Load} is the load resistance. Assuming no switching loss, the output power equals to P_{rated}. Consequently, R_{Load} is determined as $(V_{out})^2/P_{rated}$.

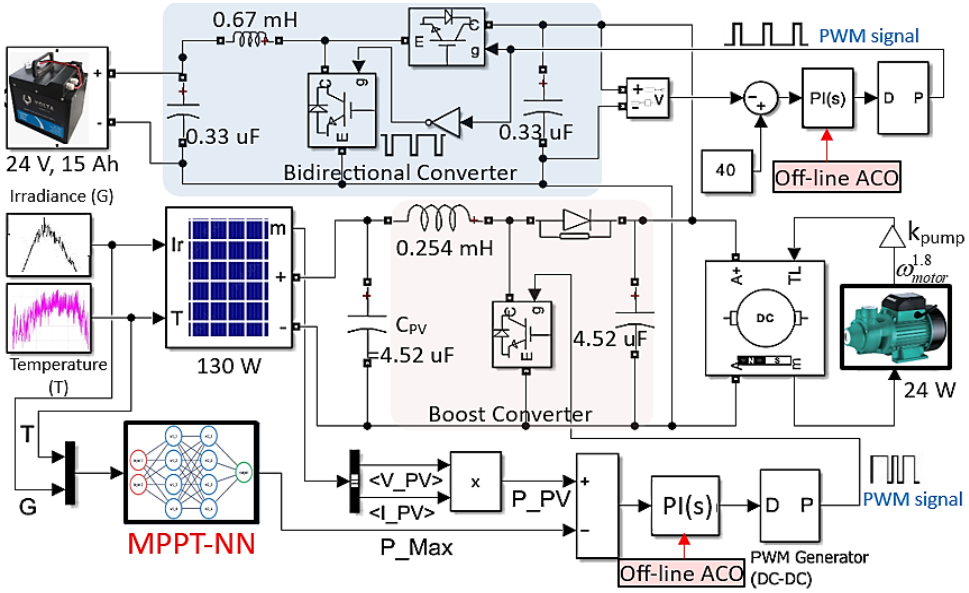

Figure 2 PV pumping system with controllers simulated in Matlab/Simulink

In a bidirectional converter or charger design, buck mode (charge) is activated when the boost voltage output at the DC bus ($V_{DC\text{-}bus}$) exceeds the referenced DC bus voltage ($V_{ref,DC\text{-}bus}$), and vice versa, boost mode (discharge) is employed, enabling the battery management. The minimum inductance of charger ($L_{min,charger}$) is determined by (1) like the inductance of boost converter by let V_{in} = $V_{DC\text{-}bus}$, V_{out} = V_{bat} (rated battery voltage), while the minimum conductance of the charger ($C_{min,charger}$) is as follows [30].

$$L_{min,boost} = L_{min,charger} = \frac{V_{in} \times (V_{out} - V_{in})}{f_{sw} \times \Delta I_{ripple} \times V_{out}}, \quad (1)$$

$$C_{min,boost} = \frac{P_{rated} \times (V_{out} - V_{in})}{\Delta V_{ripple} \times f_{sw} \times V_{out}^2}, \quad (2)$$

$$C_{min,charger} = \frac{\Delta I_{ripple}}{8 \times f_{sw} \times \Delta V_{ripple}}, \quad (3)$$

where ΔI_{ripple} = $\%_{Iripple} \times I_L \times V_{out}/V_{in}$, and ΔV_{ripple} = $\%_{Vripple} \times V_{out}$, $\%_{Iripple}$ is current ripple percentage, $\%_{Vripple}$ is voltage ripple percentage, and f_{sw} is switching frequency.

For V_{in} at 17.4 V (voltage at MPP), 10% ripple voltage and current, and f_{sw}= 20 kHz, the design results in $L_{min,boost}$ = 0.254 mH and $C_{min,boost}$= 4.52 µF, (Figure 2). For V_{in} = 40 V ($V_{DC\text{-}bus}$) and V_{out} = 24 V (battery voltage, V_{bat}), the design results in $L_{min,charger}$ = 0.672 mH, and two $C_{min,charger}$ = 0.33 µF each, (Figure 2).

The implemented circuit (Figure 3), component values closely resemble those in the simulations. For converter circuits (Figure 3), selected boost inductance, L_{boost} = 0.275 mH, selected boost capacitance, C_{boost} = 4.7 µF, selected bidirectional charger inductance $L_{charger}$ = 1 mH, and selected bidirectional capacitor, $C_{charger}$ = 50 µF. Both circuits utilize a P600 diode with a 600 V voltage tolerance and an IRF540N MOSFET Switch rated at 62.5 kHz for up to 100 V and 33 A tolerant.

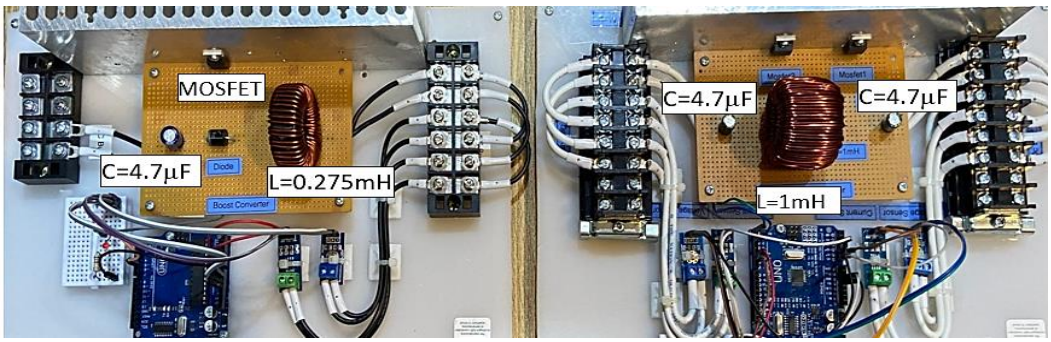

Figure 3 Implemented boost (left) and bidirectional (right) converters

The PV panel, a SHARP ND-130T1J model, which comprises 32 cells per module with specifications: PV power at MPP (P_{MPP}) = 130 W, PV voltage at MPP (V_{MPP}) = 17.4 V, PV current at MPP (I_{MPP}) = 7.48 A, PV open-circuit volage (V_{OC}) = 22 V, and PV short-circuit current (I_{SC}) = 8.09 A, is used. PV panel conversion efficiency, typically below 30%, can decrease significantly due to variations in G and T, particularly affecting the MPPs (Figure 4(a) and (b)). This results in notable efficiency degradation, especially when connected to a motor-pump, causing power losses from mismatched operating points (green line, Figure 4(a)).

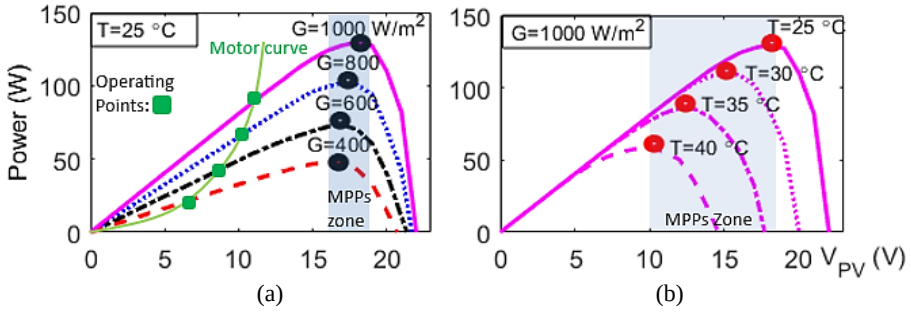

Figure 4 Motor curve with the operating points and MPP deviations due to variations in (a) irradiance (*G*) and (b) temperature (*T*)

2.1 Controller design

The proposed NN-based MPPT for the boost converter stage is shown in Figure 5.

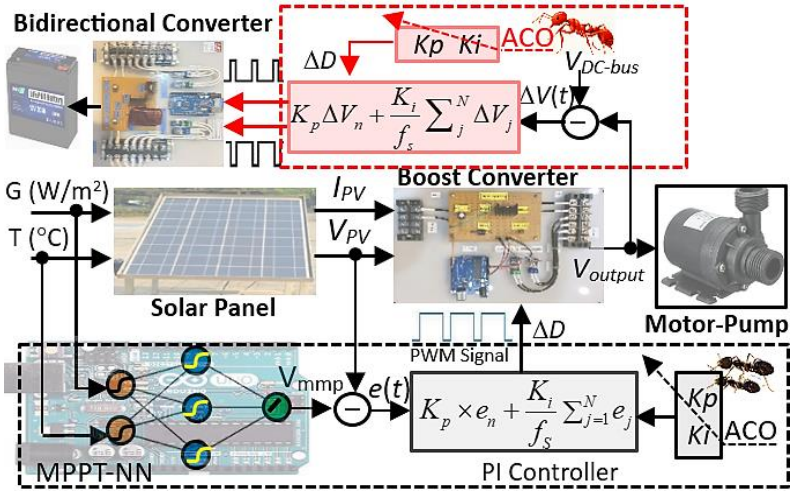

Figure 5 MPPT-NN and PI controller (black-dashed-box), along with an additional PI charger-controller (red-dashed-box), all tuned using ACO

The NN has three layers: a 2-node input layer for *G* and *T*, an *M*-node hidden layer with nonlinear processing using a hyperbolic tangent activation function (tanh), and an output node for V_{MPP} with a linear function *f*,

$$V_{MMP} = f\left(\sum w_{h-o}\left(\tanh\left(\sum_M w_{i-h}G + ww_{i-h}T + b_{i-h}\right) + b_{h-o}\right)\right), \quad (4)$$

where $\{w_{i-h}, ww_{i-h}, b_{i-h}\}$ and $\{w_{h-o}, b_{h-o}\}$ are the weights' and biases' coefficients between input-hidden and hidden-output layers, respectively, and *f* is linear function.

The training datasets are acquired by solving the PV current and voltage (I_{PV}, V_{PV}) points from implicit (5) to determine V_{MPP} and MPPs under (*G*, *T*) conditions. Equation (5) requires 5 PV parameters of the used PV panel, including photocurrent (I_{ph}), diode saturated current (I_s), ideality factor (*n*), shunt resistance (R_p), and series resistance (R_s), all of which are taken following the method referred to in [31]. Here, we conduct an experiment to extract these parameters using pseudo-irradiance (Figure 6(c)), resulting in I_{ph} = 8.11 A, I_s = 2.4×10^{-10} A, *n* = 1.1, R_p = 96.15 Ω, and R_s = 0.26 Ω.

$$I_{pv} = K\left[I_{ph} - I_s\left(\exp(qV_{Rp}/nK_BT_1) - 1\right)\right] - V_{Rp}/R_p, \quad (5)$$

where $K = (G_2/G_1)[1 + \alpha(T_2 - T_1)]$, $V_{Rp} = V_{PV} + I_{PV}R_S$, α=0.048, K_B is Boltzmann constant, q=1.6×10^{-19}, and standard test condition of G_1=1000 W/m^2 and T_1 = 298 K.

Over 1000 collected datasets (Figure 6(a)) from solving (5) with inputs of {*G*, *T*} and target of V_{MPP} are split into 60% for training and 40% for testing. The MPPT-NN's performance is evaluated using root mean square error (RMSE). Optimal 3 hidden nodes (*M*) (Figure 6(c)), corresponding 13 coefficients of *w*'s and *b*'s are determined, and the optimal MPPT-NN is expressed in (6) without black-box modeling, facilitating implementation in microcontrollers.

$$V_{MPP} = f\left(\begin{Bmatrix} -0.33 \times \tanh(-2.36 \times G - 0.57 \times T + 2.42) \\ +0.89 \times \tanh(-1.29 \times G - 2.05 \times T) \\ -0.77 \times \tanh(1.87 \times G + 1.54 \times T + 2.42) \end{Bmatrix} + 0.83\right). \quad (6)$$

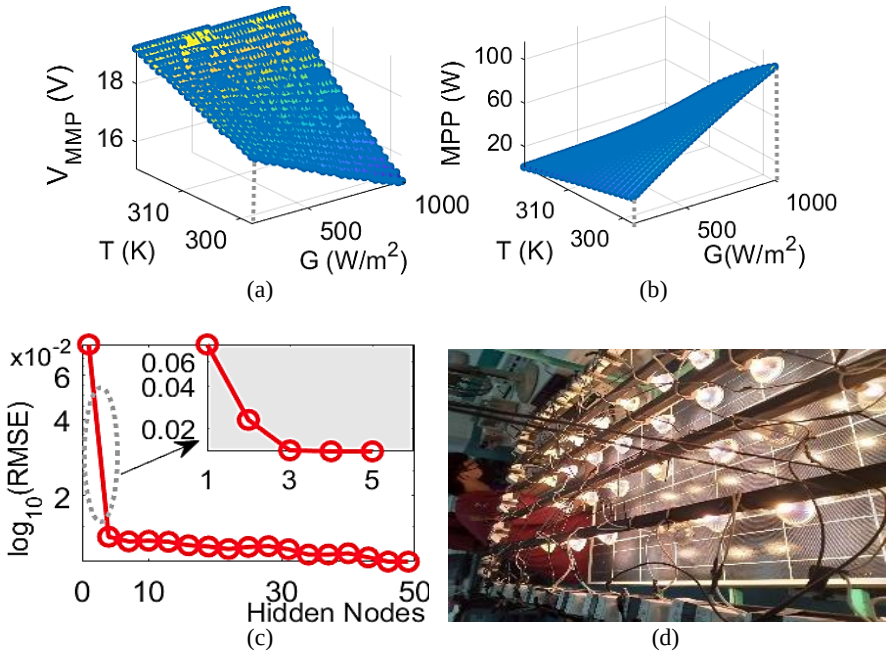

Figure 6 (a) Collected datasets of inputs {*G*, *T*} and target of V_{MPP}, (b) corresponding MPPs, (c) Hidden nodes versus RMSE, and (d) Experimental pseudo-irradiance setup for extracting the PV parameters

2.2 Controller's parameters optimization

ACO, a population-based soft-computing method, effectively optimizes controller parameters by mimicking ants finding food [32]. Real ants share information via pheromones to find the optimal path from nest to food, analogous to how artificial ants navigate optimal solutions through ACO, reducing the computational effort. Unlike exhaustive trial-and-error methods, such as for manually adjusting PI gains by initially setting integral parameter (K_i) to a large value and then finding proportional gain (K_p) followed by fixing K_p and adjusting K_i, ACO provides a more systematic approach. On the other hand, traditional approaches based on selecting the damping ratio of quadratic equations require an exact mathematical model of the system, resulting in fixed PI gains that perform well only within a limited operational range. Here, ACO is employed to simultaneously fine-tune the PI gains in the MPPT stage (7) and in the charge stage (8) for the boost and bidirectional converters, respectively.

$$\Delta D_{Boost} = K_{p,Boost} e_n + K_{i,Boost} \sum_{j=1}^{N} e_j T_s, \tag{7}$$

$$\Delta D_{Charger} = K_{p,charge} \Delta V_n + K_{i,charge} \sum_{j=1}^{N} \Delta V_j T_s, \tag{8}$$

where $e_n = V_{mpp} - V_{PV}$, $\Delta V = V_{DC\text{-}bus} - V_{output}$, and $T_s = 1/f_s$ is a sampling period.

The predefined search domain of K_p's $\in [10^{-4}, 0.5]$ and K_i's $\in [10^{-2}, 1]$ obtained from pilot experiments is evenly divided into 100 grid nodes (K_{p1}, K_{p2}, …, K_{p100} and K_{i1}, K_{i2}, …, K_{i100}) (Figure 7(a)), with step sizes of 4.9×10^{-3} and 9.9×10^{-3}, resulting in possible 100×100×100 tours. Initially, artificial *M* ants are randomly distributed among nodes, and k^{th} ant starts its tour from node *i* to any node *j* (denoted by the same color, Figure 7(a)) guided by transfer probability (P_{ij}) (9) determined by an updated pheromone parameter (τ_{ij}) (10) deposited by others and a heuristic function $\eta_{ij} = |f_{obj,j}(\theta) - f_{obj,i}(\theta)|^{-1}$, representing the inverse of the difference in the integral of the square error (ISE) as the objective function f_{obj} in discrete form (11).

$$P_{ij}^{k}(t) = \frac{(\tau_{ij})^{\alpha}(\eta_{ij})^{\beta}}{\sum_{i \in N_i} (\tau_{ij})^{\alpha}(\eta_{ij})^{\beta}}, \; j \in N_i, \tag{9}$$

where

$$\tau_{ij} \leftarrow (1-\rho)\tau_{ij} + \sum_{k=1}^{M} \Delta\tau_{ij}^{k}, \tag{10}$$

$$J = \underset{\theta}{\operatorname{argmin}} f_{obj}(x) = \underset{K_P, K_I}{\operatorname{argmin}} |\sum e(t)^2 + \sum (\Delta V(t))^2|, \tag{11}$$

α and β are convergence control parameters, N_i represents the set of unvisited node points, $\rho \in [0, 1]$ is the rate of pheromone evaporation, helping in escaping local optima, and $\Delta\tau_{ij}$ denotes the incremental pheromone.

The test uses 100 iterations (tours) with 10 artificial ants, and α = 2 and β = -2. ACO converges toward near-optimal solutions, in minimizing J (11), shown in Figure 7(b).

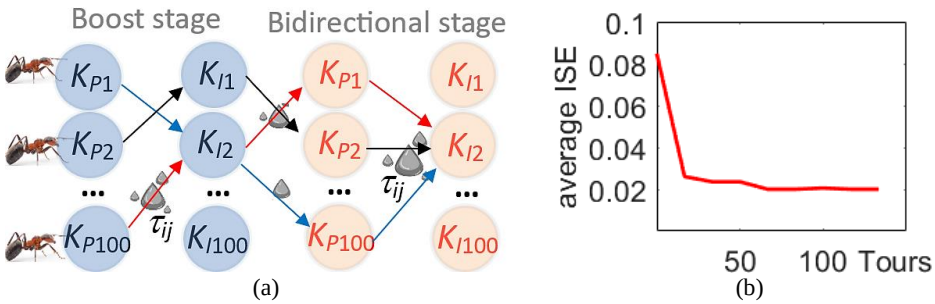

Figure 7 (a) Representation of ACO for searching K_p's and K_i's gain, and (b) Convergence of PI controller's gains

3. Results and discussion

The optimized PI gains using ACO and human tuning are shown in Table 1. The efficiency enhancement of the MPPT-NN-PI/ACO controller outperforms that of the MPPT-NN-PI using trial-and-error in both the MPPT and charger stages, providing faster transient responses and more accurate steady-state responses. In the MPPT stage (Figure 8(a)), the duty ratio generated by the proposed NN-PI/ACO controller (blue line) exhibits a significant reduction in rise time, enabling the system to reach the MPP more rapidly than the trial-and-error tuned PI controller (red line). This rapid response is crucial for maximizing energy capture from the PV panels, particularly under rapidly changing irradiance conditions.

Correspondingly, the voltage error at MPP for the NN-PI/ACO in Figure 8(b) is also significantly reduced. This improvement indicates that the system can more precisely track the optimal operating point, thereby enhancing overall energy conversion efficiency. The reduction in voltage error signifies a more accurate and stable MPPT operation, leading to better performance and reliability of the PV system.

In the bidirectional charge stage (Figure 8(c)), the duty ratio generated by both the PI/ACO and PI controllers effectively reduces oscillations. Oscillations in the control system can lead to inefficiencies such as increased thermal stress on power switches and higher heat losses. By minimizing these oscillations, the PI controllers ensure smoother operation, reducing thermal load and extending the lifespan of the DC-bus capacitor. However, the PI-ACO controller further reduces DC-bus voltage errors compared to the PI controller, which is critical for maintaining the stability and reliability of the power conversion process. Lower voltage errors mean that the DC bus voltage remains closer to the desired set point, ensuring more effective management of power flow between the PV panels, batteries, and load. This stability is vital for ensuring uninterrupted operation, especially in off-grid applications where consistency is paramount.

Table 1 Comparison of PI gains: human tuning and ACO

Converter stage	Trial-and-Error		ACO	
	Kp	***Ki***	***Kp***	***Ki***
Boost stage	1.95×10^{-2}	0.018	4.36×10^{-3}	0.4754
Bidirectional stage	1.54×10^{-4}	0.0319	1.74×10^{-4}	0.0222

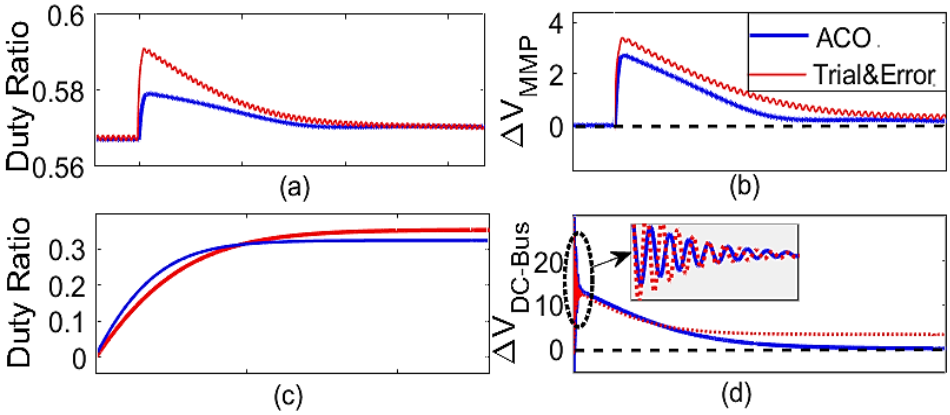

Figure 8 Step response of duty ratio with (a)-(b) V_{MPP} error (ΔV_{MPP}) for boost stage and (c)-(d) DC-bus voltage error ($\Delta V_{DC\text{-}Bus}$) for bidirectional charger stage, comparing trial-and-error with ACO-tuned PI gain

The PV-powered motor-pump system is tested during varying daytime conditions of {G, T} corresponding to their MPPs (Figure 9). Most conditions, MPPT performance is indicated by well-aligned voltage at the MPPs (Figure 10(a)). However, during the morning hours between 9:00 and 10:00 with very low irradiance, the tracked PV voltages exhibit significant oscillations around the V_{MPP}. This indicates that the NN is encountering difficulties with data not included in its training set, leading to suboptimal tracking performance during these specific conditions. Despite this, the output boost voltages at the DC-bus align well with the referenced voltage of 40 V across all weather conditions (Figure 10(b)). This consistent performance highlights the effectiveness of the bidirectional converter in maintaining stable DC bus voltage.

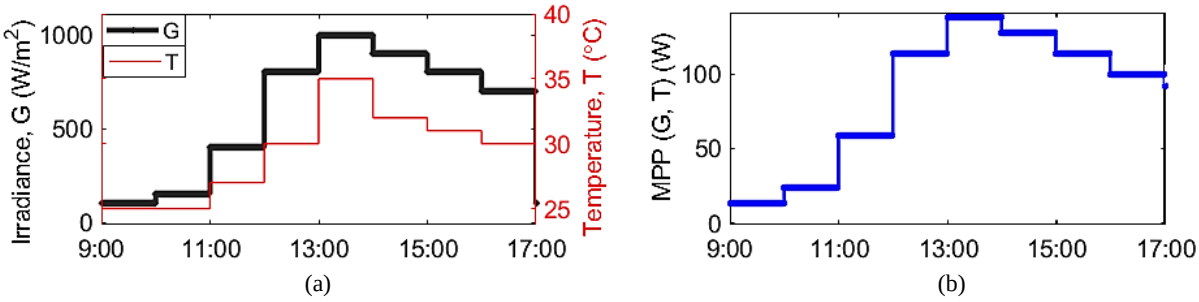

Figure 9 (a) All-day operating profile of solar irradiance (G) in W/m^2 and temperature (T) in °C, (b) Corresponding MPPs in W

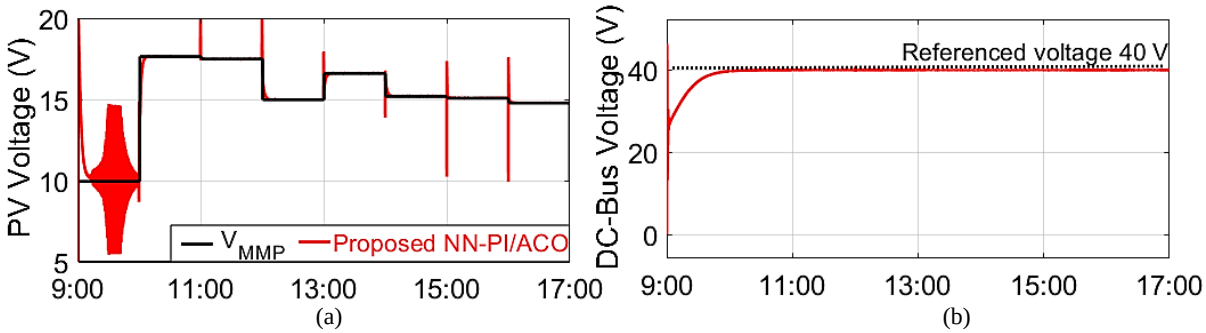

Figure 10 A comparison of (a) PV voltage tracking using MPPT-NN (red) with actual V_{MPP}, and (b) Output boost volage at the DC-bus compared to the referenced 40 V

During the period from 9:00 to 10:00, the output voltage falls below 40 V, triggering the bidirectional converter to operate in boost mode. This mode draw energy from the battery to supply the motor-pump, as indicated by the positive current flow from 9:00 to 11:00 (Figure 11(a)). This period corresponds to the battery discharging state, leading to a decline in the state of charge (%SoC) (Figure 11(b)). Conversely, from 11:00 onwards, the negative current indicates an excess of PV energy, which charges the battery. This charging process pushes the battery voltage towards its limit of around 26 V, resulting in nearly 100% SOC. This high state of charge ensures that the PV-powered motor-pump system can continue to operate at night, thus meeting the requirement for continuous 24-hour operation.

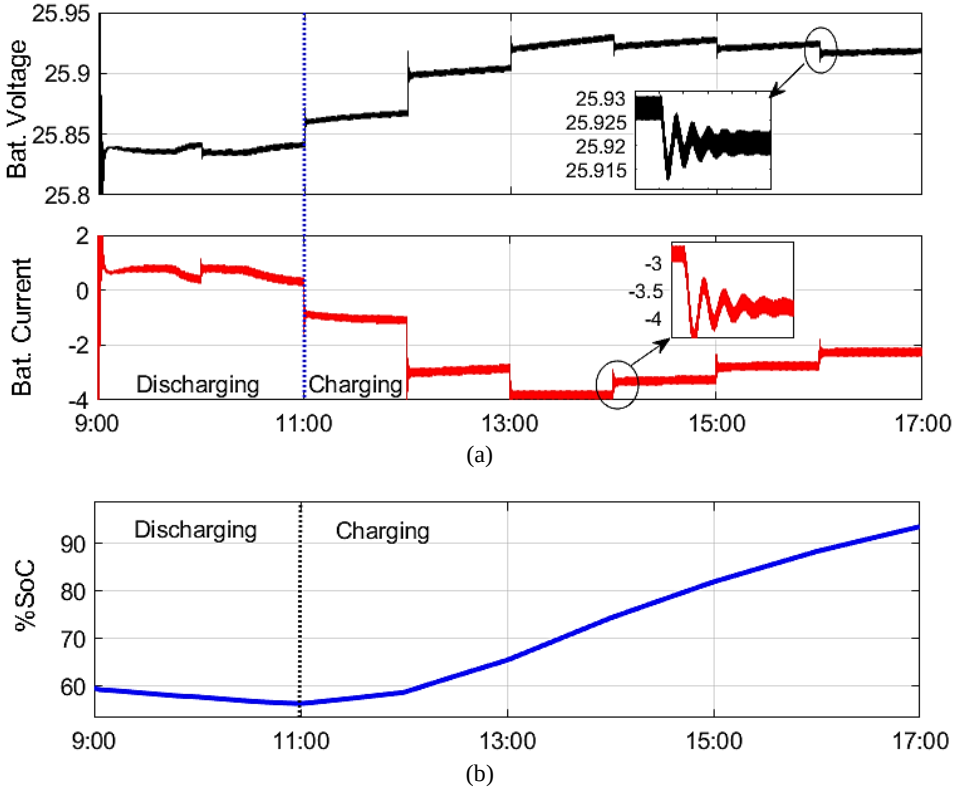

Figure 11 Control charge-discharge results: (a) Charging voltage (top) and current (bottom), (b) SoC percentage

To quantify the performance of the proposed MPPT-NN with PI controller, the energy utilization efficiency (η_{eff}) is calculated as the ratio of tracked power to the MPPs. This is averaged for each G and T condition (Figure 12), resulting in 73% and 90% efficiency for human and ACO-tuned parameters, respectively.

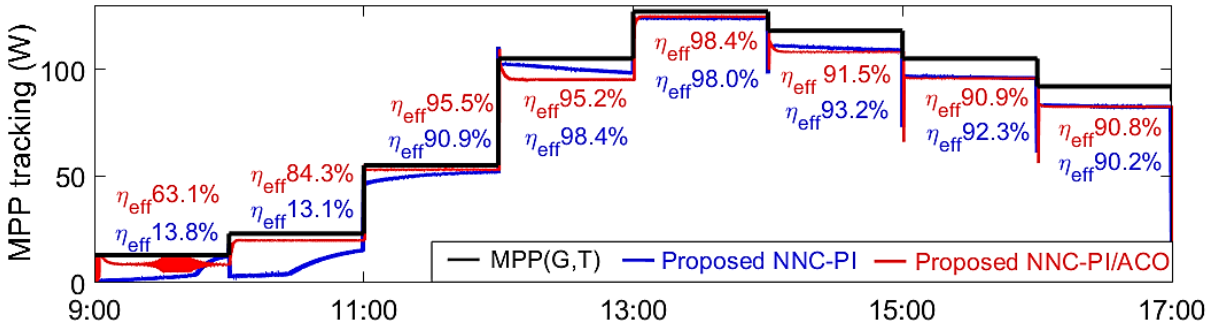

Figure 12 Comparison of energy utilization efficiency (η_{eff}) of the MPPT-NN with PI controllers tuning between human and ACO

The dynamic MPPT performance of the proposed controllers compared to other existing MPPT-controllers was examined under different weather conditions. Under high solar irradiance (Figure 13(a)), the proposed NN-PI/ACO controller demonstrates a rapid rise to the MPP without overshoot, indicating a highly responsive system. It experiences less oscillation during the transient phase than the modified P&O (MP&O) [17] and the proposed NN-PI controller, suggesting effective damping characteristics. In contrast, the Mamdani-FLC (MFLC) utilizing a triangular membership function (TMF) and tuned simultaneously with the fuzzy rules by a multi-objective genetic algorithm (MOGA), denoted as MFLC-TMF/MOGA, [18] and the optimized Takagi-Sugeno FIS-based NFC tuned by MOGA [19], show no oscillation but have a longer rise time compared to the proposed controllers. At steady-state, the proposed controllers maintain a stable output with negligible oscillations around the MPP, comparable to the performance of advanced controllers like the MFLC-TMF/MOGA and NFC. This stability ensures consistent power delivery and reduces the likelihood of wear and tear on the system components. Under low solar irradiance (Figure 13(b)), the MP&O exhibits significant overshoot and prolonged oscillations, which can lead to inefficient energy utilization and increased thermal stress on the components. It tracks the MPP incorrectly, as evidenced by the high-frequency oscillations at steady-state. These oscillations can cause significant power fluctuations, resulting in increased heat losses and reduced system efficiency. The proposed NNC-PI/ACO controller, however, shows minimal fluctuations during the transient phase and achieves a stable steady-state, indicating robustness even under challenging conditions.

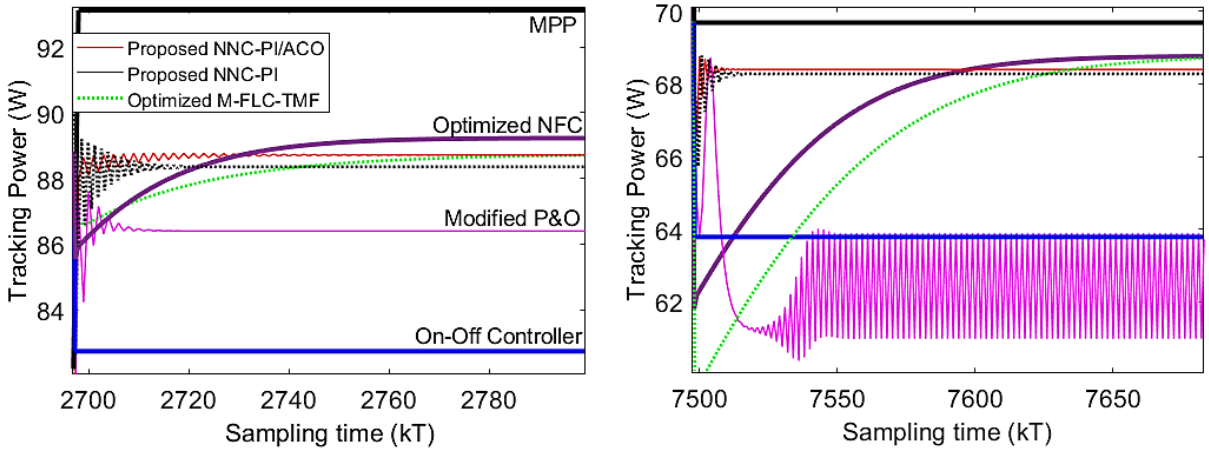

(a) High solar irradiance (b) Low solar irradiance

Figure 13 Comparison of transient and steady-state responses for MPPT between the proposed NNC-PI/ACO controller and other existing controllers under different weather conditions.

In comparing the performance of MPPT controllers (Table 2), our proposed MPPT-controller demonstrates significant improvements over various conventional and advanced controllers. Specifically, our controller achieves η_{eff} approximately 20% higher than the commercial practical on-off controller, which has an efficiency of 70% [19]. When compared to conventional controllers such as the MP&O with an efficiency of 75.7% [17], our proposed controller outperforms it by approximately 14.5%. Furthermore, in comparison to non-optimized neural network-based controllers (NNC) with an efficiency of 81% and optimized NNC using hybrid MOGA and back-propagation (*h*MOGA/BPA) [20] with an efficiency of 86%, our proposed controller still shows an improvement of about 4% to 9%.

Regarding FLCs, our proposed controller surpasses the conventional MFLC utilizing a TMF tuned manually [18, 33] with an efficiency of 85%, and the conventional MFLC using Gaussian membership function (GMF) [33] with an efficiency of 83%, by approximately 5% to 7%. However, when compared to the optimized FLC-TMF, which reduces fuzzy rules by 24% using MOGA [18] and achieves an efficiency of 91%, our proposed controller shows a slight inferiority of about 1%. Finally, the NFC based on the Takagi-Sugeno FIS and NFC-MOGA [19], with an efficiency of 95.7% and 96%, respectively, outperform the proposed NN-PI/ACO by about 6%, indicating its superior performance over the aforementioned controllers.

Table 2 Comparison of MPPT performance of existing controllers with the proposed MPPT-NN/PI-ACO controller

MPPT-based controller	Optimization method	Energy utilization efficiency (η_{eff})
The proposed NN-PI/ACO	ACO	90%
The proposed NN-PI	-	73%
Commercial on/off controller [19]	-	70%
Modified P&O [17]	-	75.7%
Conventional NNC [20]	-	81%
Optimized NNC [20]	*h*MOGA/BPA	83%
Conventional M-FLC-TMF [18, 33]	-	85%
Conventional M-FLC-GMF [33]	-	83%
Optimized M-FLC-TMF [18]	MOGA	91%
NFC [19]	-	95.7%
Optimized NFC [19]	MOGA	96%

The performance of the motor-pump system under different controllers was evaluated to assess its ability to maintain desired operating conditions (Figure 14). The speed of the motor increases from an initial stop to a constant level, ensuring that water demand is met throughout the operating period. This steady performance indicates the effectiveness of the proposed control system in maintaining operational stability despite fluctuations in weather conditions. The motor speed, as depicted in Figure 14(a), ramps up from a standstill to the desired level and remains constant throughout the operation. This consistent speed is crucial for meeting water demand reliably. The presence of small, acceptable oscillations during changes in weather conditions demonstrates the controller's ability to adapt to environmental variations while maintaining overall stability.

Additionally, the motor torque and current remain constant, as shown in Figures 14(b) and 14(c), respectively. This constancy is indicative of the controller's proficiency in managing the power requirements of the motor-pump system, ensuring efficient and uninterrupted operation. The stability in torque and current also suggests that the system is effectively handling the varying load conditions without significant fluctuations, which is essential for the longevity and reliability of the motor-pump system.

These results collectively highlight the robustness of the proposed controller in maintaining the desired motor speed, torque, and current levels, even under varying weather conditions. The system's ability to achieve and sustain operational stability with minimal oscillations underscores its potential for reliable and efficient water pumping in off-grid applications.

However, in real tests, the solar irradiance and temperature are not constant over time; they fluctuate. This requires the PV capacitor (C_{PV}) (see Figure 2) to maintain the PV voltage and current a while for controller decision-making. Subsequent a prototype solar water pump system and testing (Figure 15) revealed satisfactory operation under specified conditions, albeit with potential efficiency limitations due to equipment imperfections.

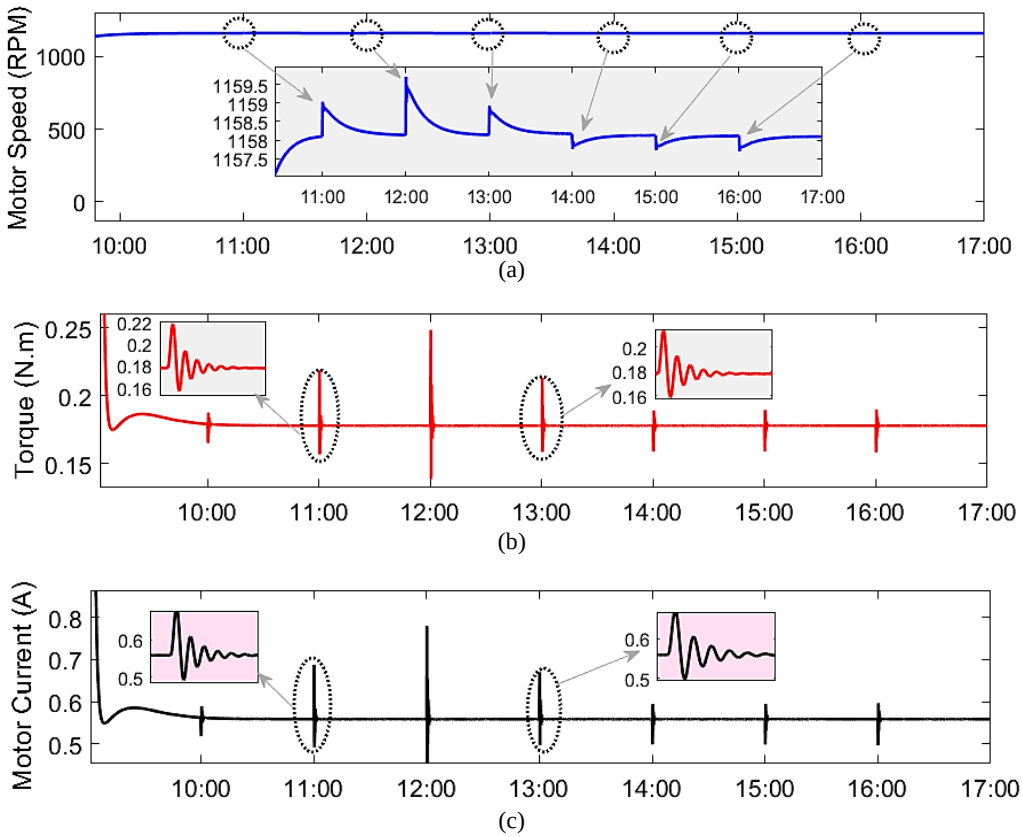

Figure 14 Control motor-pump results of the proposed controllers (a) Motor speed, (b) Motor torque, and (c) Armature current

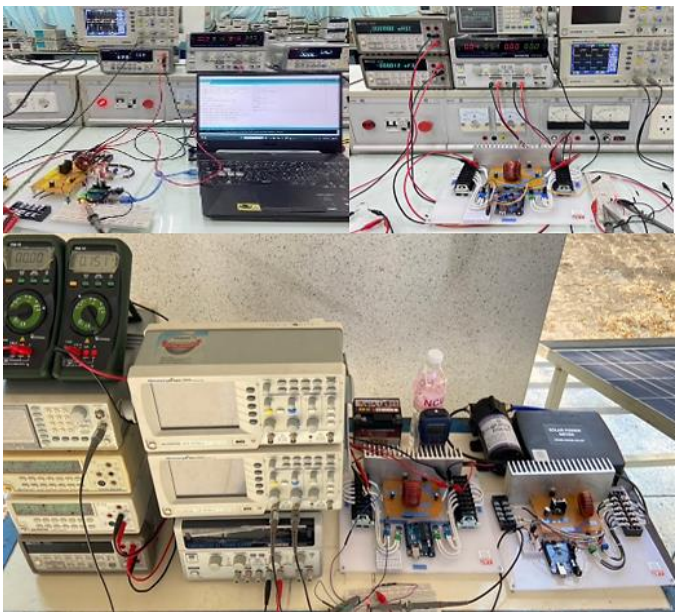

Figure 15 Equipment setup for a prototype solar water pumping system tested under laboratory and real weather conditions

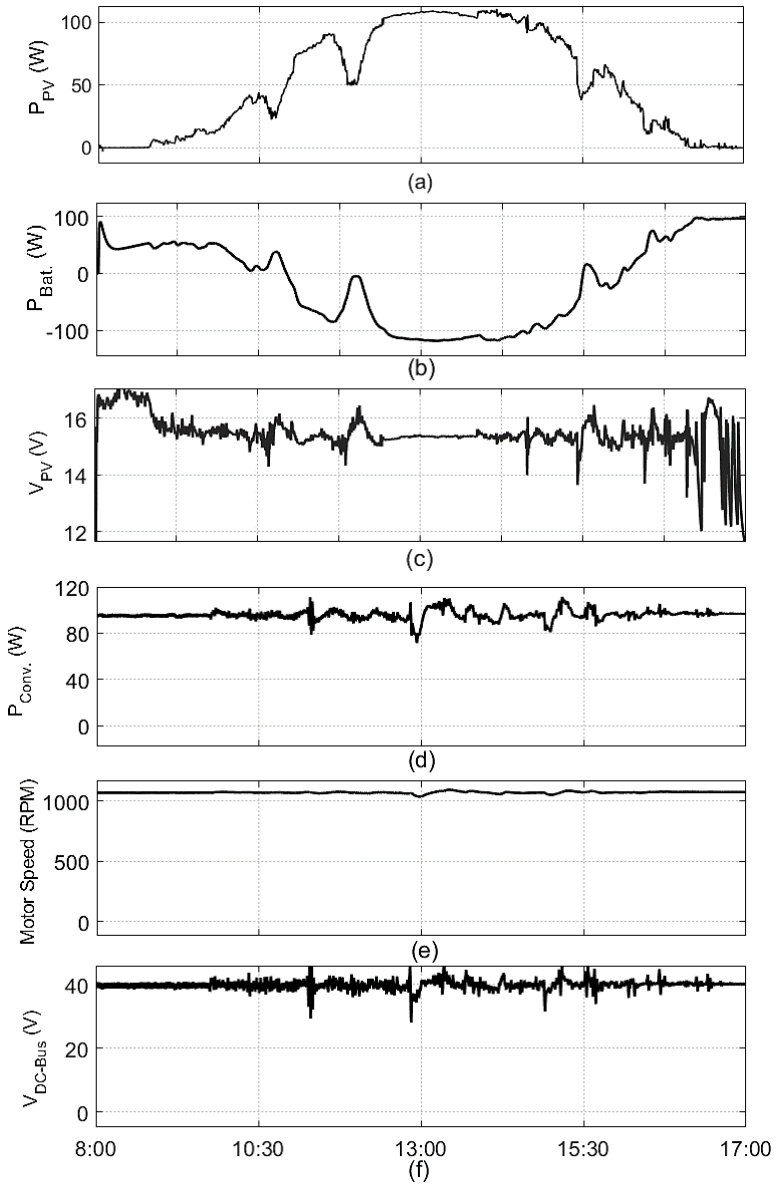

Figure 16 Experimental results of the prototype PV water pumping system

The experimental results, recorded every 30 seconds, are shown in Figure 16. The PV power output fluctuates significantly during cloudy weather (Figure 16(a)). The maximum PV power extracted by the MPPT-NN-PI/ACO controller at peak irradiance of 980 W/m² at 12:00 PM is approximately 100 W, which is 23% lower than the 130 W MPP of the PV panel used. This reduction can be attributed to power electronics losses and the high ambient temperature exceeding 40 degrees Celsius during the summer time in Thailand, which negatively impacts the PV energy conversion efficiency.

Between 8:00 AM and 11:00 AM, the system draws energy from the battery to compensate for the low PV power, ensuring uninterrupted operation (Figure 16(b)). Post 11:00 AM, excess PV power is utilized to charge the battery, demonstrating the system's effective bidirectional charge management.

The operating points of the PV panels are controlled to track the MPPs, which vary with solar irradiance and ambient temperature (Figure 16(c)). The PV voltage stabilizes when irradiance is constant, indicating the controller's efficiency in maintaining optimal operating conditions. Despite the converter delivering nearly 100 W, it falls short of the PV panel's 130 W capacity due to switching losses and decreased PV energy conversion efficiency under high ambient temperatures (Figure 16(d)). This highlights the impact of environmental conditions on system performance. The motor-pump maintains operation even during periods of low PV power in the morning, evening, and under cloudy conditions at 12:00 PM and 3:30 PM, owing to the effective bidirectional charge management. The energy stored in the batteries from 10:30 AM to 4:00 PM, amounting to approximately 450 Wh, is sufficient for nighttime operation, which requires 350 Wh. This ensures the system's reliability and continuity. The motor speed exhibits slight fluctuations around 1000 RPM (Figure 16(e)), indicating a generally stable performance with minor variations due to changing power inputs. The PI-ACO controller effectively maintains the DC bus voltage at the referenced 40 V (Figure 16(f). In instances where the output voltage drops below this value, the additional PI-ACO controller activates to discharge energy from the battery, ensuring continuous power supply to the motor-pump.

These experimental results validate the proposed system's capability to efficiently manage power fluctuations, maintain stable operation, and ensure reliable performance under varying weather conditions. The integration of MPPT-NN with PI/ACO controllers demonstrates significant improvements in energy utilization and system stability, confirming the robustness and effectiveness of the developed off-grid PV-powered motor-pump system.

4. Conclusions

This study developed an efficient off-grid PV-powered motor-pump system using a two-stage power converter, which includes a boost converter, an MPPT-NN with PI controller, and a bidirectional PI charger. Electrical components such as, inductors, capacitors, diodes, battery capacity, motor-pump selection, and power electronic switches, were theoretically designed to minimize current-voltage ripples while maintaining cost-effectiveness for small-scale systems requiring continuous 24-hour operation. Optimized by ACO, the proposed PI controller outperforms the traditional PI controller in both the MPPT and charger stages, offering faster response times, reduced voltage errors, and minimized oscillations. These improvements lead to enhance energy utilization efficiency by 17% over traditional trial-and-error tuned methods. Performance comparisons showed superior results compared to existing techniques, including commercial on-off controllers and modified P&O algorithms, and were comparable to fuzzy logic and neuro-fuzzy controllers. The system maintained a stable DC bus voltage between the boost converter and bidirectional converter, and effectively managed the battery SOC under varying conditions, ensuring optimal charging and discharging cycles. These results were validated through MATLAB/Simulink simulations and laboratory-scale prototyping, confirming the system's robustness and efficiency.

5. References

[1] Hassan QF. Solar powered water pumping system for a rural village. Ecol Eng Environ Technol. 2023;24(2):214-23.
[2] Priyadarshi N, Maroti PK, Hussien MG. Extensive performance investigation of Luo converter-based modified firefly maximum point tracking algorithm for permanent magnet snychronous motor-driven photovoltaic pumping system. IET Renew Power Gener. 2022:1-11.
[3] Priyadarshi N, Maroti PK, Azam F, Hussien MG. An improved Z-source inverter-based sensorless induction motor-driven photovoltaic water pumping with Takagi–Sugeno fuzzy MPPT. IET Renew Power Gener. 2022:1-14.
[4] Priyadarshi N, Bhaskar MS, Padmanaban S, Blaabjerg F, Azam F. New CUK–SEPIC converter based photovoltaic power system with hybrid GSA–PSO algorithm employing MPPT for water pumping applications. IET Power Electron. 2020;13(13):2824-30.
[5] Priyadarshi N, Padmanaban S, Bhaskar MS, Azam F, Khan B, Hussien MG. A novel hybrid grey wolf optimized fuzzy logic control based photovoltaic water pumping system. IET Renew Power Gener. 2022:1-12.
[6] Sukanya Satapathy S, Kumar N. Framework of maximum power point tracking for solar PV panel using WSPS technique. IET Renew Power Gener. 2020;14(10):1668-76.
[7] Wonsathan R, Seedadan I, Puangmanee W. Design and simulation of PV-powered motor-pump recirculating water system in rice filed crab farm using MPPT-based Neuro-fuzzy and bidirectional converter charger controllers. Suranaree J Sci Technol. 2024;31(3):1-10.
[8] Kumar N, Singh HK, Niwareeba R. Adaptive control technique for portable solar powered EV charging adapter to operate in remote location. IEEE Open J Circuits Syst. 2023;4:115-25.
[9] Priyadarshi N, Padmanaba S, Holm-Nielsen JB, Blaabjeg F, Bhaskar MS. An experimental estimation of hybrid ANFIS-PSO-based MPPT for PV grid integration under fluctuating sun irradiance. IEEE Syst J. 2020;14(1):1218-29.
[10] Priyadarshi N, Padmanaban S, Kiran Maroti P, Sharma A. An extensive practical investigation of FPSO-based MPPT for grid integrated PV system under variable operating conditions with anti-islanding protection. IEEE Syst J. 2019;13(2):1861-71.
[11] Errouha M, Motahhir S, Combe Q, Derouich A, El Ghzizal A. Fuzzy-PI controller for photovoltaic water pumping systems. The 7th International Renewable and Sustainable Energy Conference (IRSEC); 2019 Nov 27-30; Agadir, Morocco. USA: IEEE; 2019. p. 1-6.
[12] Satapathy SS, Kumar N. Modulated perturb and observe maximum power point tracking algorithm for solar PV energy conversion system; The 3rd International Conference on Recent Developments in Control, Automation & Power Engineering (RDCAPE); 2019 Oct 10-11; Noida, India. USA: IEEE; 2019. p. 345-50.
[13] Kumar N, Saxena V, Singh B, Panigrahi BK. Power quality improved grid-interfaced PV-assisted onboard EV charging infrastructure for smart households consumers. IEEE Trans Consum Electron. 2023;69(4):1091-100.

[14] Allahabadi S, Iman-Eini H, Farhangi S. Fast artificial neural network-based method for estimation of the global maximum power point in photovoltaic systems. IEEE Trans Ind Electron. 2022;69(6):5879-88.
[15] Belaroussi O, Ammar A, Lechelah A. Maximum power point tracking of solar water pumping systems using fuzzy logic algorithm. The 1st National Conference on Green Energy (NCGE' 2023); 2023 Dec 2; Boumerde, Algeria. p. 204-8.
[16] Kumar N. EV charging adapter to operate with isolated pillar top solar panels in remote locations. IEEE Trans Energy Convers. 2024;39(1):29-36.
[17] Tawanna N, Takkabutr F, Kesutha A, Wongsathan R, Nuangnit A, Wongsinlapamorakot N. Improvement performances of PV water pumping system using MPPT-based modified P&O controller: modeling, setting experimental package and analysis. J KMUTNB. 2021;31(1):5-15.
[18] Tawanna N, Takkabutr F, Kesutha A, Wongsathan R. Maximizing efficiency of photovoltaic water pumping system using the MPPT-based fuzzy logic controller. Suranaree J Sci Technol. 2020;27(4):1-10.
[19] Wongsathan R, Nuangnit A. Optimal hybrid neuro-fuzzy based controller using MOGA for Photovoltaic (PV) battery charging system. Int J Control Autom Syst. 2018;16(6):3036-46.
[20] Wongsathan R, Patchaiyo R, Seedadan I. MPPT-based optimal NNC-hMOGA/BPA for photovoltaic water pumping system. Int J Electr Energy. 2019;7(2):51-7.
[21] Kumar N, Saxena V, Singh B, Panigrahi BK. Intuitive control technique for grid connected partially shaded solar PV-based distributed generating system. IET Renew Power Gener. 2020;14(4):600-7.
[22] Priyadarshi N, Bhaskar MS, Almakhles D. A novel hybrid whale optimization algorithm differential evolution algorithm-based maximum power point tracking employed wind energy conversion systems for water pumping applications: practical realization. IEEE Trans Ind Electron. 2024;71(2):1641-52.
[23] Massaq Z. Design of high-performance fuzzy-predictive controllers for a photovoltaic/battery pumping system. Int J Renew Energy Res. 2023;13(1):454-65.
[24] Sharma U, Singh B, Kumar S. A smart solar water pumping system with bidirectional power flow capabilities. IEEE 7th Power India International Conference (PIICON); 2016 Nov 25-27; Bikaner, India. USA: IEEE; 2016. p. 1-6.
[25] Selmy M, El sherif MZ, Noah MS, Abdelqawee IM. Standalone PV-based water pumping system optimization using Jellyfish technique. Eng Res J. 2023;52(1):94-100.
[26] Hussien AM, Kim J, Alkuhayli A, Alharbi M, Hasanien HM, Tostado-Véliz M, et al. Adaptive PI control strategy for optimal microgrid autonomous operation. Sustainability. 2022;14(22):1-22.
[27] Bakır H, Merabet A, Kiehbadroudinezhad M. Optimized control of a hybrid water pumping system integrated with solar photovoltaic and battery storage: towards sustainable and green water-power supply. Energies. 2023;16(3):1-16.
[28] Hamidia F, Abbadi A. Improved hybrid pumping system with storage battery based on particle swarm algorithm. Rev Roum Sci Techn. 2021;66(4):243-8.
[29] Colorni A, Dorigo M, Maniezzo V. Distributed optimization by ant colonies. Proceedings of the European Conference on Artificial Life, ECAL'91; 1991 Dec 11-13; Paris, France. Cambridge: MIT Press; 1992. p. 134-42.
[30] Babu SS, Chary SSK, Abdullah SM, Elangovan D, Thundil Karuppa Raj R. Design and analysis of power convertors for electric vehicle application. IOP Conf Ser: Earth Environ Sci. 2019;312:1-12.
[31] Wongsathan R, Seedadan I. Artificial intelligence and ANFIS reduced rule for equivalent parameter estimation of PV module on various weather conditions utilized for MPPT. Int J Renew Energy. 2017;12(1):37-55.
[32] Birattari M, Pellegrini P, Dorigo M. On the invariance of ant colony optimization. IEEE Trans Evol Comput. 2007;11(6):732-42.
[33] Wongsathan R. Simulation model for controlling of the photovoltaic water pumping system. UBU Eng J. 2020;13(2):156-65.